Behavioral/Cognitive

Cascades and Cognitive State: Focused Attention Incurs Subcritical Dynamics

Erik D. Fagerholm,[1] Romy Lorenz,[1] Gregory Scott,[1] Martin Dinov,[1] Peter J. Hellyer,[1] Nazanin Mirzaei,[1] Clare Leeson,[1] David W. Carmichael,[2] David J. Sharp,[1] Woodrow L. Shew,[3] and Robert Leech[1]

[1]The Computational, Cognitive and Clinical Neuroimaging Laboratory, The Centre for Neuroscience, The Division of Brain Sciences, Imperial College London, Hammersmith Hospital Campus, London W12 0NN, United Kingdom, [2]Imaging and Biophysics, UCL Institute of Child Health, London WC1N 1EH, United Kingdom, and [3]University of Arkansas, Department of Physics, Fayetteville, Arkansas 72701

The analysis of neuronal avalanches supports the hypothesis that the human cortex operates with critical neural dynamics. Here, we investigate the relationship between cascades of activity in electroencephalogram data, cognitive state, and reaction time in humans using a multimodal approach. We recruited 18 healthy volunteers for the acquisition of simultaneous electroencephalogram and functional magnetic resonance imaging during both rest and during a visuomotor cognitive task. We compared distributions of electroencephalogram-derived cascades to reference power laws for task and rest conditions. We then explored the large-scale spatial correspondence of these cascades in the simultaneously acquired functional magnetic resonance imaging data. Furthermore, we investigated whether individual variability in reaction times is associated with the amount of deviation from power law form. We found that while resting state cascades are associated with approximate power law form, the task state is associated with subcritical dynamics. Furthermore, we found that electroencephalogram cascades are related to blood oxygen level-dependent activation, predominantly in sensorimotor brain regions. Finally, we found that decreased reaction times during the task condition are associated with increased proximity to power law form of cascade distributions. These findings suggest that the resting state is associated with near-critical dynamics, in which a high dynamic range and a large repertoire of brain states may be advantageous. In contrast, a focused cognitive task induces subcritical dynamics, which is associated with a lower dynamic range, which in turn may reduce elements of interference affecting task performance.

Key words: attention; criticality; EEG; fMRI; power law

Introduction

The brain exhibits complex patterns of electrical activity across a broad spatiotemporal range (He, 2014). Experimental data, ranging from *in vitro* electrophysiology to *in vivo* fMRI, suggest that these electrical patterns occur spontaneously and propagate across diverse regions before dissipating (von der Malsburg et al., 2010). Such events are termed neuronal avalanches, due to their qualitative similarity with the sand pile collapses observed in the Bak-Tang-Wiesenfeld model (Bak et al., 1988). Characteristics of the probability size distributions of these avalanches can be used as markers of self-organized criticality (Beggs and Plenz, 2003).

There is increasing evidence for the theory that the brain displays critical or near-critical dynamics (Beggs and Timme, 2012). Criticality is an attractive framework, as it allows for a unifying description of the ways in which information flows through the brain at disparate spatiotemporal scales (Scott et al., 2014). Critical dynamics confers beneficial functional properties, such as maximized dynamic range, information transmission, and information capacity (Shew and Plenz, 2013). However, descriptions of the brain in terms of neural dynamics typically consider the brain at rest, or in states of reduced consciousness, in which supercritical dynamics has been observed (Meisel et al., 2013; Scott et al., 2014). As such, there remains a conceptual gap between the theory of neuronal avalanches and a description of the brain as a system able to efficiently process information and perform cognitive tasks, while reacting to external events (Leech et al., 2012; Cocchi et al., 2013). Given the high dynamic range associated with critical dynamics, it stands to reason that a cognitive task requiring focused attention (narrow dynamic range) may be best performed by a noncritical neural circuit (Churchland et al., 2010; He, 2013).

Recently, a study demonstrated how different macroscopic brain networks modulate critical dynamics, and also showed that task states are associated with lower metastability (Hellyer et al., 2014). In a different approach, decreased levels of metastability have been linked with deviation from criticality (Haldeman and

Beggs, 2005). This led us to predict that a focused cognitive state, such as the choice reaction task (CRT), would be associated with noncritical neural dynamics, whereas the resting brain would display hallmarks of criticality (Hellyer et al., 2014). Here we test for deviation from criticality with respect to changes in cognitive state. We measured the distance of EEG cascade size probability distributions from power law form, either during a continuous resting scan, or during blocks of CRT and intermittent rest. These cascades represent an aggregate signal across the brain, and should therefore not necessarily be considered as having the same physiological mechanisms as the neuronal avalanches observed at microscopic scales in LFP experiments (Beggs and Plenz, 2003). We also related the effects of EEG-domain cascades to spatial BOLD patterns in simultaneously recorded fMRI data, to better characterize the cascades. For example, the EEG cascades could be associated with the following: (1) the global fMRI BOLD signal, reflecting a whole-brain phenomenon; or (2) brain regions involved in high-order cognitive control; or (3) earlier sensorimotor regions. This information allows us to distinguish between different possible functional roles of the cascades. Finally, we investigate the relationship between reaction times in the CRT and proximity of cascade size probability distributions to power law form.

Materials and Methods

We provide a high-level overview of methods in Figure 1A.

Subjects

Eighteen healthy volunteers (11 males) with mean age ± SD 28.02 ± 5.44 (age range 20–41) were initially recruited for this study. Two of the 18 subjects were subsequently excluded due to incomplete data acquisition. Subjects had no history of either contraindication to MRI scanning or neurological/psychiatric disorders. All subjects were right-handed with either normal or corrected-to-normal vision. All subjects gave written informed consent and the study was approved by the Hammersmith Hospital (London, UK) research ethics committee.

EEG recording

EEG data were collected simultaneously with fMRI scanning using scanner-compatible amplifiers (BrainAmp MR; Brain Products), together with an electrode cap consisting of 30 sintered silver/silver chloride ring electrodes (BrainCap MR; Brain Products) placed according to the extended international 10–20 system (Fig. 1B; Chatrian et al., 1988; Klem et al., 1999). Hardware-based EEG/MR clock synchronization was achieved using the SyncBox device by Brain Products (Ullsperger and Debener, 2010). In addition to EEG, an EOG (one channel) and ECG (one channel) were recorded. Electrodes were referenced to FCz and a ground electrode was positioned at Iz (10–5 electrode system; Oostenveld and Praamstra, 2001). All impedances were kept below 20 kΩ. The sampling rate was set at 5 kHz with a hardware bandpass filter from 0.016 to 250 Hz.

MRI acquisition

Images were acquired using a 3.0 tesla MRI scanner (Siemens Magnetom Verio syngo MR B17) with a phased array head coil and sensitivity encoding (SENSE) with undersampling factor 2. A whole-brain EPI sequence was used (T2*-weighted gradient-echo, voxel size 3.00 × 3.00 × 3.00 mm, field of view 192 × 192 × 105 mm, flip angle 80°, TR/TE = 2000/30 ms, 35 ascending slices with 3.00 mm thickness). Magnetic field inhomogeneity within the brain was corrected using quadratic shim gradients. Whole-brain structural images (T1-weighted) were also acquired for all subjects.

Scanning conditions

All subjects underwent two separate scans: one continuous resting state (awake, eyes open) lasting 480 s, and one CRT scan lasting 520 s, with consecutive task and intermittent rest blocks lasting 49 s each. During task scans, subjects were shown a fixation cross for 350 ms, followed by an

arrow pointing in the direction of the required response for 1400 ms, with an interstimulus interval of 1750 ms. Subjects used the index fingers on each hand to respond as quickly and accurately as they were able. Tasks were presented using the MATLAB Psychophysics Toolbox (Psychtoolbox-3). Reaction times and accuracy were recorded with a custom-made response box.

Removal of MRI artifacts

Data preparation. The start of the fMRI data acquisition was identified using BrainVision Analyzer's (BrainVision recorder software; Brain Products) automatic artifact detection algorithm. This software registers rapid changes in the voltage gradient via characteristic MRI gradient-related artifacts. We inspected the quality of the automatic artifact detection and manually corrected the marker for the onset of artifact where necessary. Markers indicating each repetition time (TR) were then generated every 2 s using a BrainVision Analyzer 2.0.2 macro, and the MRI gradient synchronized with the EEG recording clocks.

MR scanner artifact correction

We then used BrainVision Analyzer's MR template subtraction to correct for MR artifacts (Allen et al., 2000). The correction algorithm computes a representative template artifact that can be subtracted from each TR window (indicated by the inserted TR markers), removing most of the MR-related noise (Eichele et al., 2010). For the initial correction template calculation we included the first five volumes, starting from the fourth TR marker (the scanner automatically discards the first three volumes to remove T1-related signal fluctuations). We used a correlation-based approach, which includes successive volumes in the correction template calculation when the similarity (correlation) of the artifact in that interval is above a certain threshold ($r > 0.975$), resulting in a clean and homogenous template (Gutberlet et al., 2009). Before the template calculation step, we performed baseline correction on the EEG data across the whole artifact-affected data. We used a finite impulse response low-pass filter at 40 Hz. As such, according to the Nyquist theorem, we capture all frequencies of interest with a sampling rate of 80 Hz. We downsampled the data to 250 Hz using BrainVision Analyzer, to allow for more than two data points per oscillation (for the Nyquist sampling frequency case). This increases our signal-to-noise ratio and therefore allows a more precise estimation of the oscillation cycle.

Cardioballistic and eye-blink artifact correction

The next step was to correct for cardioballistic (CB) artifacts using the ECG data. This was achieved by first inserting heartbeat markers into the data. For this purpose, a representative segment in the MR-corrected ECG was defined, upon which the automatic pulse-detection algorithm (BrainVision Analyzer) was based. This segment was manually chosen to be as long and clean as possible. The algorithm then found stable time points across all ECG episodes within this segment using a template-matching approach (Gutberlet et al., 2009). The resulting template was then used to detect peaks in the ECG channel throughout the rest of the dataset and corresponding heartbeat markers were inserted. The data were visually inspected and locations of the automatically created markers were adjusted to match apparent peaks in ECG events where necessary.

Next, independent component analysis (ICA) was used to correct for CB artifacts. To achieve this we ran an Infomax ICA on the same portion of clean data as used for the ECG peak detection. Based on the previously inserted heartbeat markers, the automatic CB correction parameter solution (BrainVision Analyzer) was used to identify ICs that contribute most significantly to the ECG artifact in the EEG channels (Gutberlet et al., 2009). This procedure is proposed as an alternative approach to the standard template subtraction method (Allen et al., 1998). In addition, we also identified ICs associated with eye blinks and eye movements. We then removed all ICs labeled as artifact source components before performing the inverse transformation to the data.

Motion removal and channel rejection

The clean EEG data were exported into the MATLAB-based toolbox EEGLAB and manually inspected for motion and other artifacts (Delorme and Makeig, 2004). Motion detection was performed using an automated EEGLAB procedure, which utilizes the joint probability of all
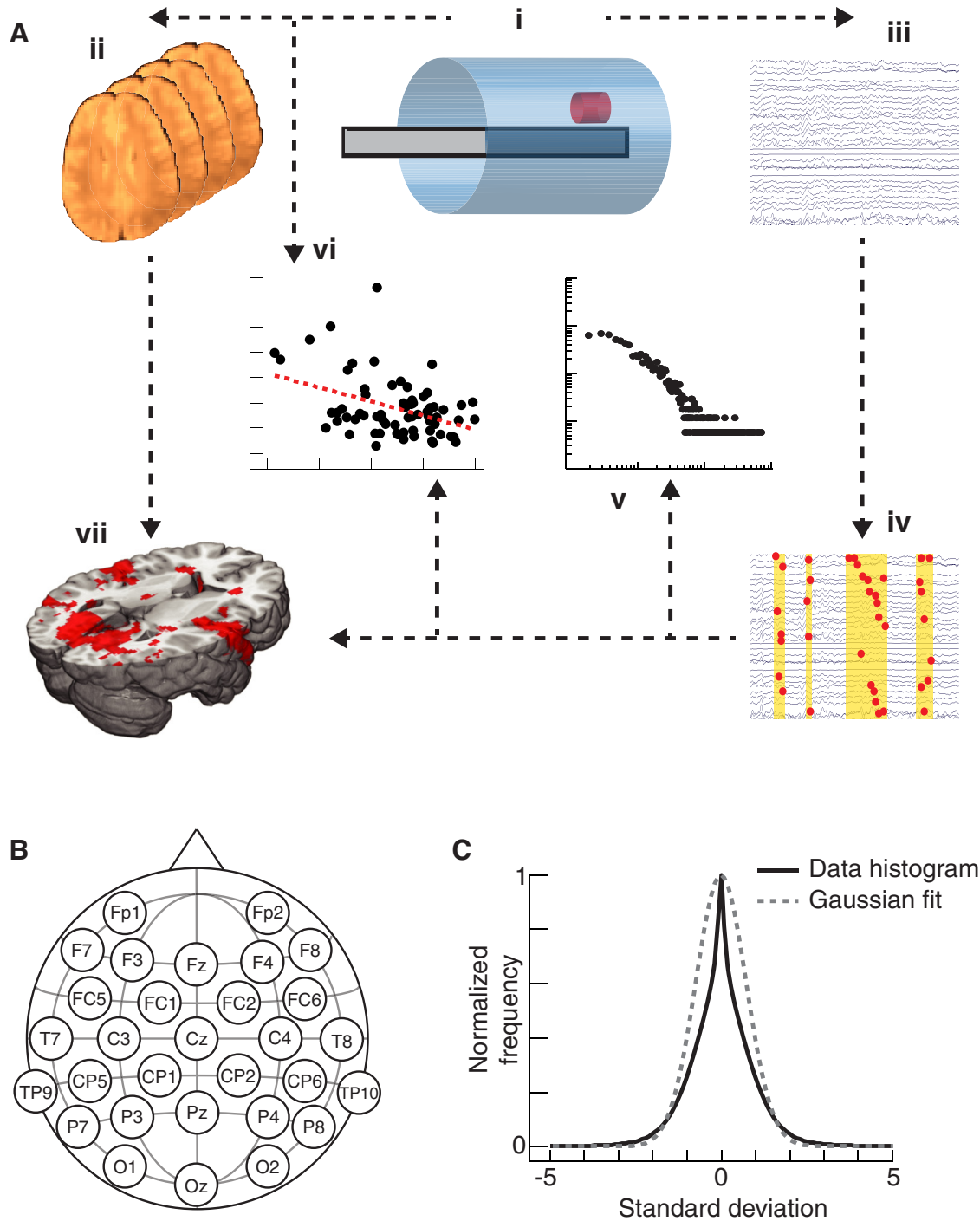
Figure 1. High-level overview of methods. ***Ai***, Simultaneous EEG and fMRI recording. ***Aii***, Preprocessing of fMRI data. ***Aiii***, Preprocessing of EEG data. ***Aiv***, Cascade detection in EEG data. ***Av***, EEG κ statistics derived across all subjects, scanning conditions, and scanning blocks. ***Avi***, EEG-derived κ statistics compared with individual reaction times in the task condition. ***Avii***, Explained variance in fMRI data due to EEG cascade timings displayed on a standard brain for group-level statistics. ***B***, EEG electrode positions. The positions of the 30 EEG electrodes on the scalp, set out according to the extended international 10 −20 system. ***C***, EEG histogram. A histogram of the z-transformed EEG data is presented, together with a fitted Gaussian distribution.

channels, with an activity probability limit of 2 SD used (based on visual inspection of the automatically marked epochs). The motion correction was repeated by hand; time points at which a large number of channels deflected concurrently with similar amplitudes were marked and excluded from subsequent analyses. All results are reported for data preprocessed with automatic motion detection, but robustness of results is confirmed for data preprocessed with manual motion exclusion. Artifactual channels were removed based first on visual inspection and then based on automatic detection, using the joint probability of the recorded electrode with a detection threshold of 5 SD.

Artifact-corrected EEG data were then high-pass filtered at 0.1 Hz before analysis to remove low-frequency components (such as electrogalvanic signal). The time courses for each of the 30 EEG channels were then z-transformed (mean subtraction and division by the SD), with the motion artifact segments removed before the z-transform to prevent spurious offsets in the data.

EEG time-course shuffling
To validate the results, we generated a null hypothesis dataset that preserved temporal information but not spatiotemporal information in the

EEG dataset. To do this, we generated datasets in which the individual EEG channel time courses had been temporally shuffled using random-offset circular permutation following preprocessing. All analyses were rerun using these shuffled time courses to demonstrate that the results are not an artifact of data with a certain power spectrum. We then generated shuffled time courses of the "raw" EEG data in the same way and ran these through the same preprocessing steps as described above. All analyses were rerun using these shuffled time courses to demonstrate that the preprocessing is not responsible for the results observed in the non-shuffled data. All relevant results are reported for data that had been shuffled before preprocessing, with qualitatively similar results confirmed for data shuffled post preprocessing.

EEG cascades

Cascades in the EEG data were detected using the method described previously (Meisel et al., 2013). We thresholded the z-transformed absolute value time course of each channel at greater than a certain SD and then binarized the result. Results are presented using a threshold of 2.0 SD, selected by examining the data histogram (Fig. 1C) relative to its fitted Gaussian distribution (Meisel et al., 2013). All subsequent results are consistent between 1.0 and 2.5 SD. Fewer than 1% of deflections appear above 2.5 SD, resulting in a large number of distributions with finite-size bias in the fit of a power law distributional model (Clauset et al., 2009); i.e., the statistical power to detect differences between scanning conditions decreases. Furthermore, all results are reported using time windows of 8 ms, with results remaining consistent between 4 and 12 ms.

The binarized time courses were then summed across all 30 channels to give a 1D time course that measures the total number of channels for which the absolute-value activity lies above the given threshold at each time point. Following Meisel et al. (2013), this single time course was then binned into time windows of a certain size. The duration of a cascade was then defined as a continuous period of nonzero bins in between two zero (quiescent) bins. The size of a cascade was defined as the sum of all bins comprising the cascade. EEG cascade detection was performed separately for each subject, scanning condition, and scan block. Our approach, following that of Meisel et al. (2013), differs from investigations of neuronal avalanches at the microscopic level, in which both spatial as well as temporal information are used to define avalanches (Beggs and Plenz, 2003). This is because the exact neural source of scalp-recorded EEG information is technically difficult to localize. Equally, from a theoretical perspective, the existence of long-range white-matter tracts means that simple Euclidean representation of space may not be appropriate when considering macroscopic data measured across the scalp.

Cascade statistics

Cascade-size probability distributions were calculated by counting the frequency of cascade sizes and dividing each frequency by the total number of cascades. This was done separately for each subject, scanning condition (continuous rest, task, and intermittent rest), and scan block. Probability distributions with insufficient data points were excluded from subsequent analysis, as determined by the presence of a finite-size bias in the fit of a power law distributional model (Clauset et al., 2009). We assessed how far a given distribution lies from that of a system operating at criticality by calculating the distance between the curves of a given cumulative probability distribution of cascade sizes and a reference power law (Shew et al., 2009; Yang et al., 2012). This results in a quantity, κ, which is equal to 1.0 for a critical system, <1.0 for a subcritical system, and >1.0 for a supercritical system. All relevant results are reported for reference curves using an exponent of −1.5, with qualitatively similar results confirmed for the exponent range −1.8 to −1.2. The maximum of the reference power law was set at the maximum observed cascade size for each examined probability distribution (one for each scanning condition, subject, and scanning block). All results are reported using a reference power law minimum size calculated at 0.1% of the maximum observed cascade size for each examined probability distribution. Qualitatively similar results were confirmed using a range of possible minima for the reference power law of each examined distribution. The "floor" of this range was set after the initial "bump" in each probability distribution

(giving an approximate cascade size in the range of 4–7), as these are more likely to correspond to noise in the data. Similarly, the "ceiling" of this range was set at 1% of the maximum of each distribution, in order not to remove excessive amounts of data. κ was computed separately for both the resting state and CRT scans (split into task and intermittent rest blocks) for all subjects. It is possible to produce values of κ that lie spuriously close to unity if the data distribution crosses the reference distribution. As such, any distribution for which the absolute value of the distance between data and reference curves exceeded the nonabsolute value was rejected from subsequent analyses. The continuous rest data were split into segments of equal duration (49 s) before cascade detection, to match the duration of the task and intermittent resting blocks, therefore avoiding bias in the collection of cascade statistics. Cascades that occur during times of possible motion, as detailed above, were excluded from all subsequent statistics.

Cascade shapes

In addition to analyzing the sizes of cascades, we also used the algorithm described previously (Meisel et al., 2013) to track the size of a given individual cascade at every time point throughout its duration. We were thereby able to obtain the average sizes of all cascades of different durations at all time points for the three scanning conditions (continuous rest, task, and intermittent rest) across all subjects. To quantify the self-similarity of cascades of different durations, we collapsed the data by rescaling the sizes and durations, as described previously (Friedman et al., 2012). We quantified the extent to which the cascade shapes overlap by fitting splines to the rescaled plots (normalized between zero and unity). We then calculated the distance between these rescaled shapes at linearly spaced data points and divided the total distance by the number of data sites used (100 across all analyses). We calculated these distances for shapes of various durations and divided by the number of shapes under comparison. For example, if we wish to quantify the extent of self-similarity of three shapes of durations a–c, then

$$\mathcal{F}_{total} = \frac{100}{3}(\mathcal{F}_{ab} + \mathcal{F}_{ac} + \mathcal{F}_{bc}),$$

i.e., 100% for perfect data collapse.

MRI preprocessing

All fMRI data were preprocessed using FSL FEAT (Smith et al., 2004). Structural and functional brain images were separated from nonbrain tissue using the FSL brain extraction tool and visually checked using FSLview (Smith, 2002). The effect of motion between scans was corrected via realignment of EPI images during the preprocessing stage using MCFLIRT (Jenkinson et al., 2002). Spatial smoothing was performed using a 5 mm full-width at half-maximum Gaussian kernel. Further, EPI data were high-pass filtered at a cutoff frequency of 0.01 Hz to correct baseline signal drifts. Boundary-based registration was used to register individual EPI functional data to individual T1-weighted structural images (Greve and Fischl, 2009). Subsequently, images were linearly registered to a standard brain atlas (MNI) using FLIRT (Jenkinson and Smith, 2001). To correct for non-neural sources of noise, time courses for CSF (MNI: 2, 10, 8) and white matter (MNI: −26, −22, 28) were removed from the datasets using least-squares linear regression.

Standard fMRI contrast analysis

We followed the standard FSL FEAT GLM to determine the effect of CRT on BOLD activation. We entered block CRT timings as regressors in FEAT, convolved with synthetic HRFs (double-gamma HRF) and added motion parameters, estimated using MCFLIRT (6D motion parameters) and FSL motion outliers as nuisance regressors. We then analyzed the fMRI data with respect to the two contrasts of task>rest and rest>task. The resulting individual subject-level parameter estimates were then entered into a high-level (mixed-effects) cluster-corrected FEAT analysis. The analysis of group effects was performed using local analysis of mixed effects (FLAME) using mean relative root mean squared (rms) motion parameters as confound regressors for validation of results in the absence of subject-level motion. All final group-level images were thresholded using a cluster correction threshold of $Z > 2.3$ and a cluster significance

threshold of $p < 0.05$. Group-level images were visualized on an average surface brain using MRICron (Rorden and Brett, 2000).

EEG-informed imaging analysis

In the next part of the study we examined the way in which EEG cascades relate to activation at the spatiotemporal scale measured by fMRI. At the subject level, statistical analyses were performed in FSL FILM using random effects GLMs with local autocorrelation correction by voxelwise temporal prewhitening. Design matrices were generated for the voxelwise time series analysis with double-gamma HRF functions, in addition to the first derivatives of explanatory variables (EVs) to account for temporal offsets. The timings of large EEG cascades (above a high SD trigger threshold) were entered as EVs in the GLM. We do this to quantify how much of the variance in fMRI activity can be explained solely by EEG cascades, with the effects of motion and task activation covaried from the data, as described in the following paragraph.

Cascades occurring during times of possible motion in the EEG trace were entered as confound EVs in the GLMs. In addition to EEG motion confounds, both fMRI motion parameters (six columns) and fMRI motion outliers (FSL motion outliers) were also entered into the GLM as covariates of no interest. Further, a task-block regressor was entered as a confound EV to account for mean offset effects in the difference between rest and task. This was done to prevent the GLM from falsely attributing task timing-related variance in the fMRI data to cascades in the EEG. All EVs were high-pass filtered at the same cutoff frequency as the fMRI data. The resulting individual subject-level parameter estimates were then entered into high-level (mixed-effects) cluster-corrected FEAT analyses; these investigated whether there were overall effects of EEG cascades across all three conditions and each condition individually, as well as a within-subject ANOVA, investigating differences between conditions. The analysis of group effects was performed using FLAME with mean relative rms motion parameters as confound regressors to control for any residual subject-level motion. All final group-level images were thresholded using a cluster correction threshold of $Z > 2.3$ and a cluster significance threshold of $p < 0.05$. Group-level images were visualized on an average surface brain using MRICron.

We extract EEG cascade explanatory variables using a threshold of 2 SD (results remain consistent between 2 and 4.5 SD and binning windows of 4–12 ms). Below an SD of 2, the EEG cascade time courses show very little variance, given the downsampling required to match the fMRI temporal resolution. To further test the robustness of these results, the above analysis was rerun with cascade time courses that had been generated by (1) using cascade timings with the same mean and SD of start times and durations as the empirical data; (2) using cascade timings from the empirical data, for which the start times had been shifted by ±5 s; and (3) using cascade timings generated from data in which the time courses of individual channels had been shuffled using circular permutation with random offset. None of these three methods showed any significant association with BOLD signal, which demonstrates that the results are not artifactual, but rather arise from a genuine relationship between EEG and fMRI.

Individual variability in cognitive performance

Finally, we investigated the relationship between individual subjects' reaction times during task and how far their neural dynamics operate from criticality, as quantified by κ. We calculated correlations between reaction times and κ across all participants using linear mixed-effects models to account for the multiple reaction times considered for the same subjects.

Results

Task-related functional imaging activation

Before investigating the EEG-domain cascades and their relationship to cognitive state, we first explored the fMRI data with standard contrasts to illustrate which brain regions are activated, as well as deactivated, by task. This provides a way of interpreting the spatial pattern of BOLD signal associated with the EEG-defined cascade time courses. Figure 2A demonstrates the effects of task>intermittent rest and intermittent rest>task contrasts during the CRT. The results show that, as expected, task perfor-
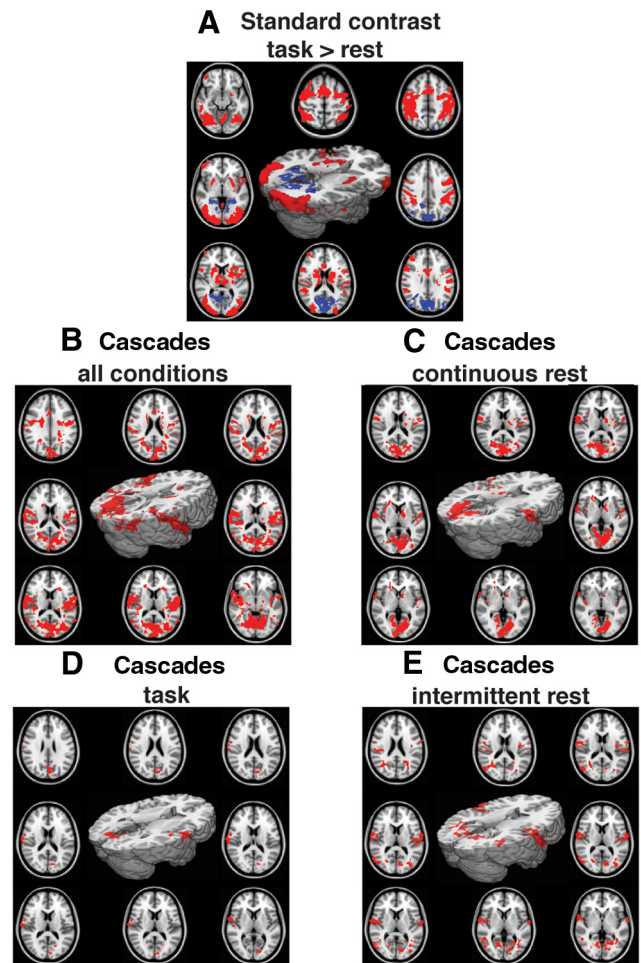

Figure 2. Spatial maps of fMRI activity. Cluster-corrected group-level statistics, with motion regressed from the data, projected onto the standard MNI 152 2 mm brain, as well as onto axial slices, for *A*–*E*. *A*, Standard contrast. CRT>rest: warm colors are voxels with relative activation, cold colors are voxels with relative deactivation. *B*, BOLD signal associated with EEG-defined cascades (using a threshold of 2 SD to define the EEG cascades). Results are combined across all three conditions: continuous rest, task, and intermittent rest. *C*, Same as *B*, but with only continuous rest data. *D*, Same as *B* but with CRT task data (significant effect of cascades is only apparent using the lower threshold, SD > 2; with higher thresholds no voxels survive multiple-comparison correction. *E*, Same as *B*, but with only intermittent rest data.

mance is associated with activation within predominantly higher order visual and motor systems, including ventral and dorsal visual streams and superior prefrontal regions, as well as within the basal ganglia (Bonnelle et al., 2011; Sharp et al., 2011). Greater activation for intermittent rest over task is observed in the medial early visual regions, as well as in the precuneus and lateral inferior parietal regions, consistent with nodes of the default mode network (DMN; Raichle et al., 2001).

Mapping EEG cascades to functional images

We next identified regions in which activation corresponded to EEG-defined cascades, by using cascade time courses to interrogate the fMRI data: providing additional information to characterize the EEG-defined cascades. Figure 2, B–E, shows brain regions for which there is significant positive correlation between the timings of EEG cascades and fMRI activity. We first investigated the effect of EEG cascades obtained from an amalgamation of data from all cognitive states on the fMRI data (Fig. 4B). These generalized cascades are associated with increased BOLD signal
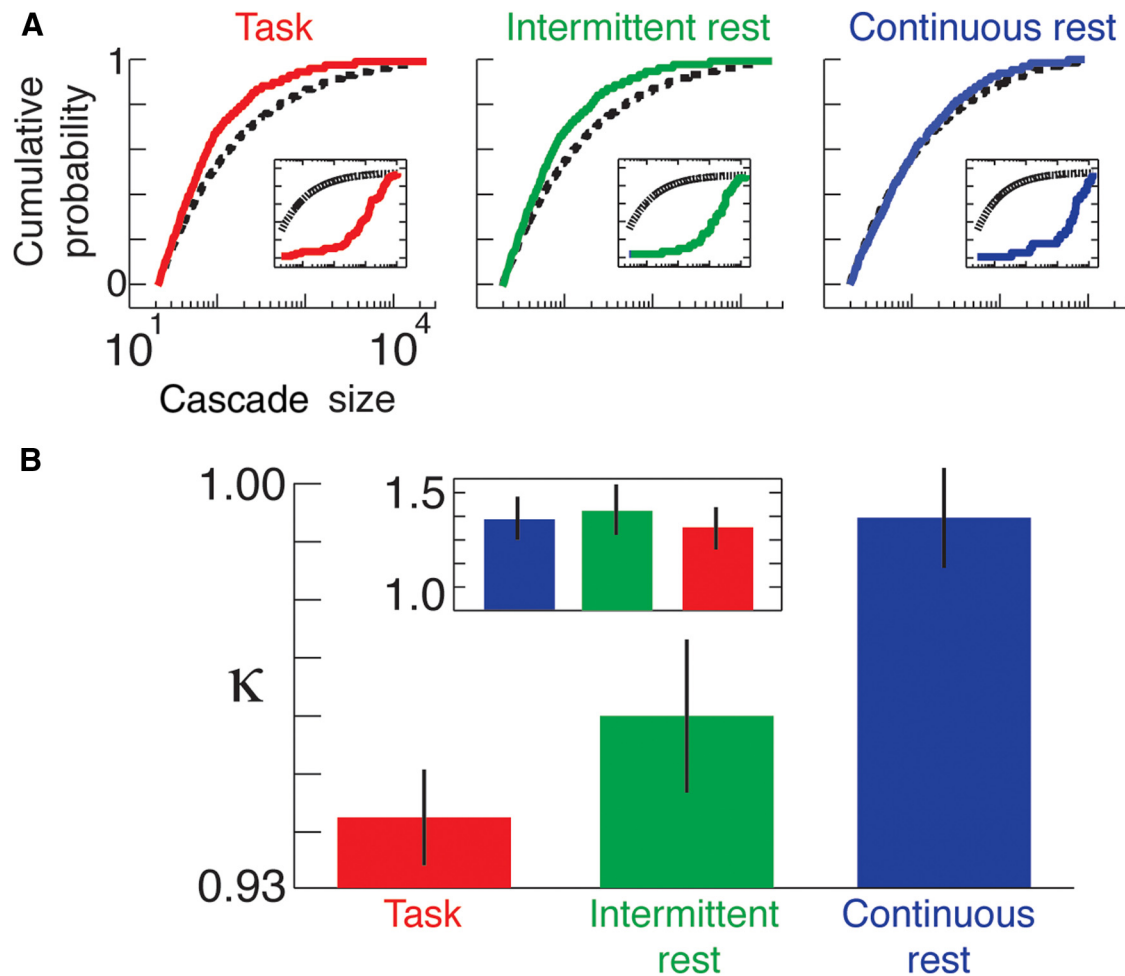
Figure 3. κ across individuals and scanning conditions. **A**, Cascade cumulative probability size distributions for an individual subject across all three scanning conditions (continuous rest, task, and intermittent rest). Reference power laws are shown by black dotted lines. Results for temporally shuffled EEG data are shown in the insets. **B**, Average values of κ for each scanning condition across all individuals; results are shown using a threshold of 2 SD but similar results are found for a range of SD threshold values. The result for temporally shuffled EEG data is shown in the inset.

predominantly in primary and adjacent auditory, visual, and somatosensory and motor regions in the superior temporal, occipital, and inferior lateral medial parietal lobes.

We then limited our analysis to EEG cascades occurring during separate cognitive states: continuous rest, task, and intermittent rest. A broadly similar set of regions to the combined conditions above was activated for cascades occurring during the continuous rest condition (spatial correlation between all conditions and continuous rest: $r = 0.89$). The spatial correspondence between all conditions and the CRT states remained high, with $r = 0.85$ and $r = 0.73$ for task and intermittent rest, respectively. However, there were only very small significant clusters of activation in the task condition and only or the SD > 2 threshold, although the spatial pattern of these clusters was similar to the other conditions. Contrasting the different conditions with repeated-measures ANOVA (continuous rest vs task vs intermittent rest) showed no significant differences. These results suggest a broadly consistent relationship between EEG cascades and the spatial patterns of the corresponding fMRI BOLD signal across task conditions.

When comparing the spatial distribution of EEG-related BOLD activation and the standard CRT contrast results, there was little if any overlap (spatial correlation between all conditions and the standard CRT BOLD results $r < 0.05$), suggesting that EEG-defined cascades (across all three conditions) involve a different set of brain regions to those that activate during the CRT task.

Cascades in different cognitive states

We proceeded by investigating the deviation of cascade distributions from power law form (measured by κ) across cognitive states. First, we established that there was no significant difference in the number of cascades between task and either the continuous or the intermittent resting state ($t_{(15)} < 0.74$, $p > 0.52$). Figure 3A shows plots of EEG cascade-size cumulative probability distributions for a single subject to illustrate the three cognitive states: continuous rest, task, and intermittent rest. We see that the continuous rest distribution more closely resembles the reference power law than the task and intermittent rest states. We also show that the cumulative distributions for the temporally shuffled EEG data do not vary across scanning conditions and do not display power law-like behavior (Fig. 3A, inset).

Figure 3B shows group-level values of κ for the three scanning conditions, revealing a significant difference between task and continuous rest across the range of parameters outlined in Materials and Methods ($F_{(1,117)} > 7.97$, $p < 0.01$), assessed using repeated measure two-way ANOVA tests. Group-level differences between continuous rest and intermittent rest, as well as between task and intermittent rest, do not remain significant across the explored parameter space. Group-level differences for the temporally shuffled EEG data were not significant between any scanning conditions for the explored parameter space ($F_{(1,117)} < 0.52$, $p > 0.48$). Subcritical dynamics ($\kappa < 1$) were evident during task,

whereas continuous rest was closer to power law form ($\kappa \approx 1$). The intermittent rest state was statistically indistinguishable from task.
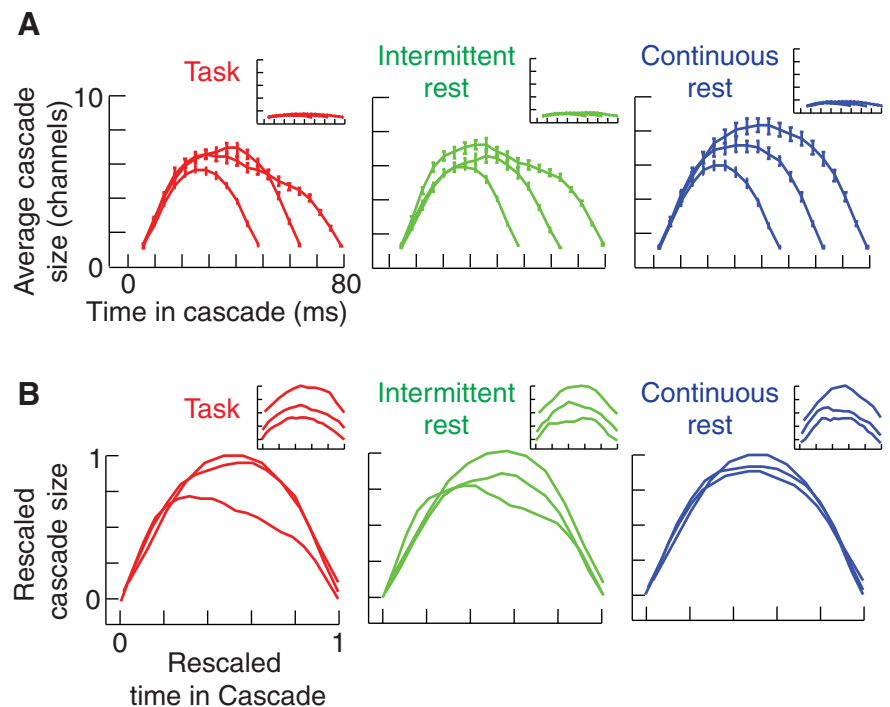
Cascade shapes

Group-level comparisons of cascades of different durations show approximately parabolic shapes for those occurring within periods of continuous rest, compared with those occurring within both task and intermittent rest (Fig. 4A). Furthermore, the continuous rest shapes collapse onto approximately the same functional form when rescaled, as opposed to the task and intermittent rest shapes (Fig. 4B; Friedman et al., 2012). The extent of overlap for the three scanning conditions was found to be $F_{\text{continuous rest}} = 95.8 \pm 1.1\%$, $F_{\text{task}} = 88.0 \pm 1.9\%$, and $F_{\text{intermittent rest}} = 89.7 \pm 1.4\%$. The extent of overlap for the temporally shuffled EEG data was found to be lower in all cases, $F_{\text{shuffled}} < 71.3 \pm 4.7\%$ (Fig. 4B, inset).

Individual variability in cognitive performance

Figure 5 shows the relationship between task κ values and reaction times for all individuals and scanning blocks (five blocks of CRT per individual). We used linear mixed-effects models to account for the repeated measurements for each subject (Aarts et al., 2014). There was a significant negative association between reaction times and κ across all explored parameters as outlined in Materials and Methods ($t_{(68)} < -3.19$, $p < 0.02$), such that reaction times decreased as κ increased from 0.9 to 1. Although reaction time was inversely proportional to κ, it should be noted that, as opposed to during the continuous rest state, task κ values were <1. There was no significant association between reaction times and κ across any explored parameters for the temporally shuffled EEG data ($t_{(55)} > -1.15$, $p > 0.25$).

Discussion

We have shown, for the first time, that EEG-domain cascades are associated with visual, auditory, and sensorimotor areas in simultaneously recorded fMRI data. We went on to show that, while the number of cascades did not change between different states, the probability distributions of cascades associated with the most focused cognitive state are indicative of subcritical dynamics. In contrast, the distributions were closer to power law form during continuous periods of rest, consistent with systems operating with near-critical dynamics. We provided further support for this possibility by showing that cascade shapes occurring during continuous resting periods collapse to scaling functions better than those occurring during either task or intermittent rest. The best behavioral performance (i.e., lower average reaction times) occurred for those individuals with cascade distributions closer to power law form. Although task was generally associated with subcritical dynamics, deviation from criticality was associated with worse performance. We discuss this seemingly counterintuitive result below, in the context of studies on optimal levels of sustained cognitive performance.

Figure 4. Cascade shapes. **A**, Average sizes of cascades across all subjects (at a threshold of 2 SD) at every time point for three different temporal scales for continuous rest, task, and intermittent rest. Results for temporally shuffled EEG data are shown in the inset. **B**, Cascade-shape curves in **A**, rescaled across both the x- and y-axis as described in Materials and Methods. Results for temporally shuffled EEG data are shown in the inset.

Despite the reported functional benefits of criticality (Kinouchi and Copelli, 2006; Shew et al., 2009; Larremore et al., 2011), we found that the more cognitively demanding task state was associated with subcritical dynamics, whereas rest was associated with near-critical dynamics. One possibility that may account for this seeming paradox is that critical dynamics are advantageous in the context of exploratory brain states, in which specific neural activity related to focused sensory input or motor output is not behaviorally relevant (Leech and Sharp, 2014). For example, in resting states, it may be advantageous for a system to possess a large dynamic range across all sensory modalities, to sensitively detect any relevant stimuli, and for resultant information to be rapidly transmitted and integrated across the brain. In contrast, the focus required for executing a specific task may be better suited to relatively low dynamic range, which is expected in a subcritical state. This interpretation is consistent with our observations both of neural dynamics with approximate power law behavior at rest and of EEG cascades generally associated with sensorimotor systems in the fMRI data.

We observed that the EEG-domain cascades map onto fMRI BOLD activation in regions associated with visual, auditory, somatosensory, and motor processing; the same system that was observed when averaging across the three conditions was also observed in the continuous and intermittent rest, as well as (less robustly) for the CRT task condition. In addition, we showed that these somatosensory regions are spatially orthogonal to those that are activated for the CRT task (using a standard fMRI only, blocked task>rest analysis). These results suggest that the EEG cascades we detected may reference a consistent set of somatosensory brain regions regardless of cognitive state (rather than regions typically associated with higher level cognitive control). We propose that what changes with different cognitive states is the distributional properties of these cascades rather than where

A

B
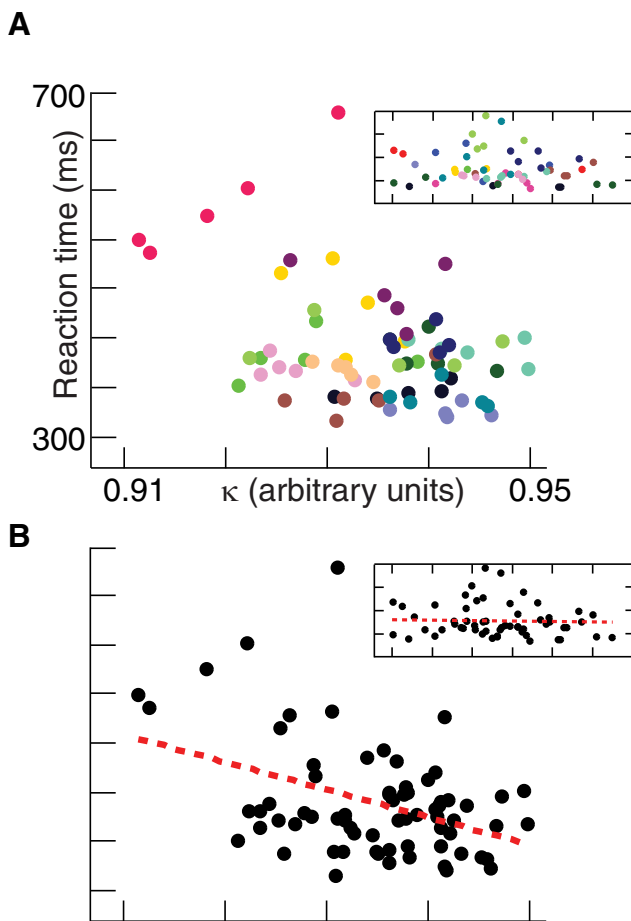
Figure 5. κ versus reaction time. **A**, Reaction times of subjects, with one value for each subject and scanning block, plotted against the corresponding EEG-derived κ values, with each individual assigned a different color. The result for temporally shuffled EEG data is shown in the inset. **B**, Same as **A**, but with best-fit regression line and the result for temporally shuffled EEG data shown in the inset.

they originate (although it is possible that more subtle differences in terms of the associated BOLD signal may exist but not be detectable with the current data. It is important to note that the EEG cascades (that are an aggregation of signals generated across the brain arriving at the scalp) will not reflect all cascades across the brain (especially regions whose cascade time courses may not be orthogonal to each other).

The resting brain may need to be able to detect and respond to information from any sensory modality (Deco et al., 2009; Leech and Sharp, 2014), resulting in a need for critical dynamics operating across sensorimotor systems. However, in the context of more active cognitive states (compared with continuous rest), a high dynamic range and maximized information transfer may not be advantageous. Focused cognitive states may require a lower dynamic range, i.e., the ability to ignore task-irrelevant information. This would promote sustained, consistent information processing, relevant only to the detection of task-related sensory input and to the performance of task-related motor output. In the context of the visually presented CRT, information processing unrelated to the task (e.g., auditory information) may interfere with task performance. As such, broad-based information processing may be detrimental in this context and subcritical dynamics advantageous. It is interesting to note that, in contrast to the subcritical dynamics observed here for a focused cognitive state, supercritical dynamics have been reported in states of reduced consciousness, such as sleep deprivation and anesthesia

(Meisel et al., 2013; Scott et al., 2014). This suggests that the relationship between cognitive state and neural dynamics lies on a spectrum, ranging from supercriticality in states of reduced arousal, to near-critical dynamics at rest, and subcriticality for focused cognitive states.

The fastest reaction times in the CRT occurred the closer the EEG cascade distributions resembled power law form, a result that may at first seem at odds with the finding that task performance was associated with subcritical dynamics. However, this result may reflect similarly counterintuitive findings that have been reported using more standard neuroimaging analyses. In particular, optimal performance (in terms of speed and accuracy) occurs when subjects are "in the zone"; a state characterized by being task focused while performing in a relatively automatic way (Esterman et al., 2013, 2014). fMRI measures of BOLD activity suggest that being in the zone is associated with increased activity in the DMN, a set of brain regions usually associated with rest, which typically deactivate during task (Raichle et al., 2001). This implies that some level of activation within the DMN is necessary for being in the zone, but that excessive deactivation leads to suboptimal task performance. In a similar way, our results reflect an in-the-zone phenomenon, where optimal behavioral performance is associated with dynamics that, while still subcritical, is close to those observed at rest. Therefore, optimal performance may occur in a (slightly) subcritical regime, but being in an overly subcritical state may be harmful to performance, possibly due to excessively restricted dynamic range and information transmission. As such, we predict that with a larger cohort of subjects, a U-shaped relationship between κ and reaction time would emerge, such that the fastest reaction times would occur at a "sweet spot" at a value of κ somewhat <1.

While the continuous rest condition consistently showed near-critical dynamics, the task condition demonstrated consistently subcritical dynamics. However, in terms of κ, the intermittent rest blocks were situated between the other two conditions (although neither consistently significantly different from continuous rest or task across the parameter space). This placement between continuous rest and task may reflect the intermediate cognitive demands of the intermittent resting state. The continuous resting state (which demonstrated near-critical dynamics), has no explicit task demands and is typically associated with "freewheeling" thought or daydreaming. In contrast, the intermittent rest periods involve some, albeit reduced, level of sustained attention, due to the motor system's preparation for rapid response in the next task block. Our results show that the similarity between this preparatory cognitive state and task may be reflected in their similar cascade distributions. Further evidence for this possibility is provided by the higher levels of self-similarity in cascade shapes of different durations for continuous rest, compared with both task and intermittent rest.

The cascades observed in this study are defined using EEG, which provides information about neural dynamics at large scales across the brain. Given that our hypothesis relates to cognitive state, which is typically thought to involve communication across large parts of the brain, EEG is an appropriate technique in this regard. The EEG cascades observed in this study may reflect similar physiological mechanisms as those underlying neuronal avalanches measured using LFP. Indeed, we (and other similar studies) observe similar characteristics with our EEG technique as with LFP experiments, such as power law-like behavior and parabolic avalanche shapes (Meisel et al., 2013). However, the measurement techniques of EEG and LFP are different in a number of ways, including in terms of spatial scale, and it is possible that the

underlying physiological mechanisms of EEG cascades and LFP neuronal avalanches are distinct. Regardless of whether the EEG cascades are large-scale homologs of neuronal avalanches, the fact that the statistics of EEG cascades change with cognitive state suggests that they reflect underlying neural dynamics.

In conclusion, we have shown that EEG-domain cascades are predominantly associated with the activation of sensorimotor systems. We have further shown that these cascades are modulated by cognitive state, such that their probability size distributions are consistent with near-critical or subcritical regimes, depending on whether an unconstrained resting state or a highly focused task state is required, respectively (Churchland et al., 2010; He, 2013). It remains an open question, for future techniques with higher spatiotemporal resolution, whether small regions of sensorimotor cortices, associated with the specific task at hand, maintain approximately critical dynamics while the remainder of the brain operates in a subcritical regime.

References

Aarts E, Verhage M, Veenvliet JV, Dolan CV, van der Sluis S (2014) A solution to dependency: using multilevel analysis to accommodate nested data. Nat Neurosci 17:491–496. CrossRef Medline

Allen PJ, Polizzi G, Krakow K, Fish DR, Lemieux L (1998) Identification of EEG events in the MR scanner: the problem of pulse artifact and a method for its subtraction. Neuroimage 8:229–239. CrossRef Medline

Allen PJ, Josephs O, Turner R (2000) A method for removing imaging artifact from continuous EEG recorded during functional MRI. Neuroimage 12:230–239. CrossRef Medline

Bak P, Tang C, Wiesenfeld K (1988) Self-organized criticality. Phys Rev A 38:364–374. CrossRef Medline

Beggs JM, Plenz D (2003) Neuronal avalanches in neocortical circuits. J Neurosci 23:11167–11177. Medline

Beggs JM, Timme N (2012) Being critical of criticality in the brain. Front Physiol 3:163. CrossRef Medline

Bonnelle V, Leech R, Kinnunen KM, Ham TE, Beckmann CF, De Boissezon X, Greenwood RJ, Sharp DJ (2011) Default mode network connectivity predicts sustained attention deficits after traumatic brain injury. J Neurosci 31:13442–13451. CrossRef Medline

Chatrian GE, Lettich E, Nelson PL (1988) Modified nomenclature for the "10%" electrode system. J Clin Neurophysiol 5:183–186. CrossRef Medline

Churchland MM, Yu BM, Cunningham JP, Sugrue LP, Cohen MR, Corrado GS, Newsome WT, Clark AM, Hosseini P, Scott BB, Bradley DC, Smith MA, Kohn A, Movshon JA, Armstrong KM, Moore T, Chang SW, Snyder LH, Lisberger SG, Priebe NJ, et al. (2010) Stimulus onset quenches neural variability: a widespread cortical phenomenon. Nat Neurosci 13:369–378. CrossRef Medline

Clauset A, Shalizi CR, Newman ME (2009) Power-law distributions in empirical data. SIAM Rev 51:661–703. CrossRef

Cocchi L, Zalesky A, Fornito A, Mattingley JB (2013) Dynamic cooperation and competition between brain systems during cognitive control. Trends Cogn Sci 17:493–501. CrossRef Medline

Deco G, Jirsa V, McIntosh AR, Sporns O, Kötter R (2009) Key role of coupling, delay, and noise in resting brain fluctuations. Proc Natl Acad Sci U S A 106:10302–10307. CrossRef Medline

Delorme A, Makeig S (2004) EEGLAB: an open source toolbox for analysis of single-trial EEG dynamics including independent component analysis. J Neurosci Methods 134:9–21. CrossRef Medline

Eichele H, Juvodden HT, Ullsperger M, Eichele T (2010) Mal-adaptation of event-related EEG responses preceding performance errors. Front Hum Neurosci 4:65. CrossRef Medline

Esterman M, Noonan SK, Rosenberg M, Degutis J (2013) In the zone or zoning out? Tracking behavioral and neural fluctuations during sustained attention. Cereb Cortex 23:2712–2723. CrossRef Medline

Esterman M, Rosenberg MD, Noonan SK (2014) Intrinsic fluctuations in sustained attention and distractor processing. J Neurosci 34:1724–1730. CrossRef Medline

Friedman N, Ito S, Brinkman BA, Shimono M, DeVille RE, Dahmen KA, Beggs JM, Butler TC (2012) Universal critical dynamics in high resolution neuronal avalanche data. Phys Rev Lett 108:208102. CrossRef Medline

Greve DN, Fischl B (2009) Accurate and robust brain image alignment using boundary-based registration. Neuroimage 48:63–72. CrossRef Medline

Gutberlet I, Debener S, Jung T-P, Makeig S (2009) Techniques of EEG recording and preprocessing. In: Quantitative EEG analysis methods and clinical applications (Tong S, Thakor NV, eds.), pp 23–49. Norwood, MA: Artech House.

Haldeman C, Beggs JM (2005) Critical branching captures activity in living neural networks and maximizes the number of metastable states. Phys Rev Lett 94:058101. CrossRef Medline

He BJ (2013) Spontaneous and task-evoked brain activity negatively interact. J Neurosci 33:4672–4682. CrossRef Medline

He BJ (2014) Scale-free brain activity: past, present, and future. Trends Cogn Sci 18:480–487. CrossRef Medline

Hellyer PJ, Shanahan M, Scott G, Wise RJ, Sharp DJ, Leech R (2014) The control of global brain dynamics: opposing actions of frontoparietal control and default mode networks on attention. J Neurosci 34:451–461. CrossRef Medline

Jenkinson M, Smith S (2001) A global optimisation method for robust affine registration of brain images. Med Image Anal 5:143–156. CrossRef Medline

Jenkinson M, Bannister P, Brady M, Smith S (2002) Improved optimization for the robust and accurate linear registration and motion correction of brain images. Neuroimage 17:825–841. CrossRef Medline

Kinouchi O, Copelli M (2006) Optimal dynamical range of excitable networks at criticality. Nat Phys 2:348–351. CrossRef

Klem GH, Lüders HO, Jasper HH, Elger C (1999) The ten-twenty electrode system of the International Federation. The International Federation of Clinical Neurophysiology. Electroencephalogr Clin Neurophysiol [Suppl 52]:3–6. Medline

Larremore DB, Shew WL, Restrepo JG (2011) Predicting criticality and dynamic range in complex networks: effects of topology. Phys Rev Lett 106:058101. CrossRef Medline

Leech R, Sharp DJ (2014) The role of the posterior cingulate cortex in cognition and disease. Brain 137:12–32. CrossRef Medline

Leech R, Braga R, Sharp DJ (2012) Echoes of the brain within the posterior cingulate cortex. J Neurosci 32:215–222. CrossRef Medline

Meisel C, Olbrich E, Shriki O, Achermann P (2013) Fading signatures of critical brain dynamics during sustained wakefulness in humans. J Neurosci 33:17363–17372. CrossRef Medline

Oostenveld R, Praamstra P (2001) The five percent electrode system for high-resolution EEG and ERP measurements. Clin Neurophysiol 112:713–719. CrossRef Medline

Raichle ME, MacLeod AM, Snyder AZ, Powers WJ, Gusnard DA, Shulman GL (2001) A default mode of brain function. Proc Natl Acad Sci U S A 98:676–682. CrossRef Medline

Rorden C, Brett M (2000) Stereotaxic display of brain lesions. Behav Neurol 12:191–200. CrossRef Medline

Scott G, Fagerholm ED, Mutoh H, Leech R, Sharp DJ, Shew WL, Knöpfel T (2014) Voltage imaging of waking mouse cortex reveals emergence of critical neuronal dynamics. J Neurosci 34:16611–16620. CrossRef Medline

Sharp DJ, Beckmann CF, Greenwood R, Kinnunen KM, Bonnelle V, De Boissezon X, Powell JH, Counsell SJ, Patel MC, Leech R (2011) Default mode network functional and structural connectivity after traumatic brain injury. Brain 134:2233–2247. CrossRef Medline

Shew WL, Plenz D (2013) The functional benefits of criticality in the cortex. Neuroscientist 19:88–100. CrossRef Medline

Shew WL, Yang H, Petermann T, Roy R, Plenz D (2009) Neuronal avalanches imply maximum dynamic range in cortical networks at criticality. J Neurosci 29:15595–15600. CrossRef Medline

Smith SM (2002) Fast robust automated brain extraction. Hum Brain Mapp 17:143–155. CrossRef Medline

Smith SM, Jenkinson M, Woolrich MW, Beckmann CF, Behrens TE, Johansen-Berg H, Bannister PR, De Luca M, Drobnjak I, Flitney DE, Niazy RK, Saunders J, Vickers J, Zhang Y, De Stefano N, Brady JM, Matthews PM (2004) Advances in functional and structural MR image analysis and implementation as FSL. Neuroimage 23 [Suppl 1]:S208–S219. CrossRef Medline

Ullsperger M, Debener S (2010) Simultaneous EEG and fMRI: recording, analysis, and application. New York: Oxford UP.

von der Malsburg C, Phillips WA, Singer W (2010) Dynamic coordination in the brain: from neurons to mind. Cambridge, MA: MIT.

Yang H, Shew WL, Roy R, Plenz D (2012) Maximal variability of phase synchrony in cortical networks with neuronal avalanches. J Neurosci 32:1061–1072. CrossRef Medline